Effect of compensation doping on the electrical and optical properties of mid-infrared type-II InAs/GaSb superlattice photodetectors*

Wang Yong-Bin(王永宾), Xu Yun(徐 云)†, Zhang Yu(张 宇),
Yu Xiu(迂 修), Song Guo-Feng(宋国峰), and Chen Liang-Hui(陈良惠)

Laboratory of Nano-Optoelectronics, Institute of Semiconductors, Chinese Academy of Sciences, Beijing 100083, *China*

(Received 27 December 2010; revised manuscript received 25 January 2011)

This paper presents a theoretical study on the electrical and optical properties of mid-infrared type-II InAs/GaSb superlattices with different beryllium concentrations in the InAs layer of the active region. Dark current, resistance-area product, absorption coefficient and quantum efficiency characteristics are thoroughly examined. The superlattice is residually n-type and it becomes slightly p-type by varying beryllium-doping concentrations, which improves its electrical performances. The optical performances remain almost unaffected with relatively low p-doping levels and begin to deteriorate with increasing p-doping density. To make a compromise between the electrical and optical performances, the photodetector with a doping concentration of 3×10^{15} cm^{-3} in the active region is believed to have the best overall performances.

Keywords: InAs/GaSb superlattices, p-doping concentration, electrical and optical properties

PACS: 73.21.Cd, 78.20.Bh **DOI:** 10.1088/1674-1056/20/6/067302

1. Introduction

Mid- and long-wavelength infrared (MWIR, LWIR) detection is of growing importance in civilian industries, military equipments and space systems. Commercially available infrared detectors in this range are Bulk InSb, mercury cadmium telluride (MCT) and quantum-well infrared detectors (QWIPs). However, they all have inherent problems with the extremely low work temperature and the fast Auger recombination in interband detectors (Bulk InSb, MCT) and the high thermal generation rate in intersubband detectors (QWIPs).

Recently, type–II InAs/GaSb superlattices has been studied extensively as a III–V-based alternative to the established HgCdTe and QWIPs materials on account of its intrinsic merits. Due to the misaligned band alignment between InAs and GaSb layers, the energy bandgap can be tailored from 3 μm to 32 μm. The larger effective mass of electrons and holes and the slower Auger recombination rate lead to lower dark current and higher operating temperature in type-II superlattices.[1−4]

The active region in pin photodetectors fabricated from InAs/GaSb materials was initially kept undoped and had a low residual background carrier concentration. The GaSb and InAs layers have p-type and n-type residual backgrounds, respectively. Depending on comparative thickness relationship between InAs and GaSb layers in superlattices, the background of the active region is likely either n-type or p-type. Through studies of Northwestern University,[5,6] doping the active region of InAs/GaSb long wavelength infrared superlattice photodiodes to make sure the background slightly p-type would improve the electrical performance.

In the present paper, we would study how the p-doping concentration of the absorbing layer works on both the electrical and optical properties of MWIR InAs/GaSb superlattice photodetectors. The superlattice structure studied here consists of 60 periods of InAs/GaSb:Be p-type region, 200 periods of InAs/GaSb active region and 60 periods of InAs:Si/GaSb n-type region and each period is built with 8 monolayer/8 monolayer (ML) InAs/GaSb layers.[7] The reference sample with the active region unintentionally doped has the n-type background through Hall measurement and its re-

*Project supported by the Natural Science Foundation of Beijing (Grant No. 4112058), the National Natural Science Foundation of China (Grant Nos. 60906027, 60906028, 61036010, and 60636030), and the Open Fund of Key Laboratory of Information Photonics and Optical Communications (Beijing University of Posts and Telecommunications), Ministry of Education of China.

†Corresponding author. E-mail: xuyun@red.semi.ac.cn

© 2011 Chinese Physical Society and IOP Publishing Ltd

duced background carrier concentration is around the level of 5×10^{14} cm^{-3}. The other samples are assumed to be p-type with different beryllium concentrations. Temperature-dependent dark current, difference resistance, absorption coefficient and quantum efficiency are calculated as a function of the absorber doping.

2. Theoretical model

To start the simulation of electrical and optical performances of the photodetector, the electronic miniband structure of type-II InAs/GaSb superlattices is first calculated through the empirical tight-binding method (ETBM) in the sp^3s^* basis. The antimony segregation in the InAs layers and Ga_xIn_{1-x} type interface are considered. Theoretical details about the ETBM model could be found in Ref. [8] and here just the simulated result will be given later.

2.1. Dark current

Assuming a neutral centre and a triangular potential barrier in the depletion region, the dark current of InAs/GaSb superlattices consists of three terms:[9,10] i) diffusion of thermally generated minority carriers from the quasi-neutral regions; ii) generation–recombination of carriers in the depletion region and iii) tunneling of carriers through the barrier, including both the trap-assisted tunneling and band-to-band tunneling. The net current can be written as

$$I = I_{\rm DIFF} + I_{\rm gr} + I_{\rm TAT} + I_{\rm BTB}. \tag{1}$$

Current due to series resistance and contribution arising from avalanche multiplication are ignored at the present model. Each counterpart of the four current density parts is given as follows:[11–13]

$$\begin{aligned} J_{\rm DIFF} &= \left((qkT)^{0.5} n_{\rm i}^2 \left(\frac{1}{N_{\rm A}}\left(\frac{\mu_{\rm e}}{\tau_{\rm e}}\right)^{0.5} + \frac{1}{N_{\rm D}}\left(\frac{\mu_{\rm h}}{\tau_{\rm h}}\right)^{0.5}\right)\right) \\ &\times \exp\left(\frac{qV}{kT} - 1\right), \end{aligned} \tag{2}$$

$$J_{\rm gr} = -\frac{qn_{\rm i}d_{\rm dep}}{\tau_{\rm gr}} \frac{\sinh(-qV/2kT)}{q(V_{\rm bi}-V)/2kT} f(b), \tag{3}$$

$$\begin{aligned} J_{\rm TAT} &= \frac{q^2 m_{\rm e} V M^2 N_{\rm t}}{8\pi\hbar^3(E_{\rm g}-E_{\rm t})} \\ &\times \exp\left(-\frac{4\sqrt{2m_{\rm e}(E_{\rm g}-E_{\rm t})^3}}{3q\hbar E}\right), \end{aligned} \tag{4}$$

$$J_{\rm BTB} = \frac{q^3 EV}{4\pi^2\hbar^2}\left(\frac{2m_{\rm e}}{E_{\rm g}}\right)^{1/2} \exp\left[-\frac{4(2m_{\rm e})^{1/2}E_{\rm g}^{3/2}}{3q\hbar E}\right], \tag{5}$$

where q is the electron charge, k is the Boltzmann constant, T is the temperature, $n_{\rm i}$ is the temperature-dependent intrinsic carrier concentration, $N_{\rm A}$ and $N_{\rm D}$ are the acceptor and donor concentrations, $\mu_{\rm e}$, $\tau_{\rm e}$ and $\mu_{\rm h}$, $\tau_{\rm h}$ are the mobility and lifetimes of electrons and holes, respectively,[14,15] V is the voltage bias of the diode and $V_{\rm bi}$ is the built-in potential, $d_{\rm dep}$ is the depletion width,[11,16] $\tau_{\rm gr}$ is the generation–recombination lifetime, $m_{\rm e}$ is the electron effective mass, $E_{\rm g}$ is the bandgap, $\hbar$ is the Planck's constant, E is the electric field in the depletion region, $N_{\rm t}$ is the activated trap density, $E_{\rm t}$ is the position of trap levels located about $E_{\rm g}/3$ below the effective conduction band edge, M^2 is a matrix element associated with the trap potential, which is assumed to be 1×10^{-23} eV$^2\cdot$cm^3 and

$$f(b) = \int_0^\infty \frac{{\rm d}x}{x^2+2bx+1}, \quad b = \exp\left(-\frac{qV}{2kT}\right). \tag{6}$$

The associated dynamic resistances are given by

$$\begin{aligned} \frac{1}{(R_0A)_{\rm DIFF}} &= \frac{q^{3/2}}{(kT)^{1/2}} n_{\rm i}^2 \left[\frac{1}{N_{\rm A}}\left(\frac{\mu_{\rm e}}{\tau_{\rm e}}\right)^{1/2} \tanh\left(\frac{d_{\rm p}}{L_{\rm e}}\right)\right. \\ &\left. + \frac{1}{N_{\rm D}}\left(\frac{\mu_{\rm h}}{\tau_{\rm h}}\right)^{1/2} \tanh\left(\frac{d_{\rm n}}{L_{\rm h}}\right)\right], \end{aligned} \tag{7}$$

$$\frac{1}{(R_0A)_{\rm gr}} = \frac{qn_{\rm i}d_{\rm dep}}{2V_{\rm bi}\tau_{\rm gr}}, \tag{8}$$

$$\begin{aligned} \frac{1}{(R_0A)_{\rm TAT}} &= \frac{2q^2m_{\rm e}M^2N_{\rm t}}{8\pi\hbar^3(E_{\rm g}-E_{\rm t})} \exp\left(-\frac{B}{\sqrt{V_{\rm bi}-V}}\right) \\ &\times \left(1+\frac{B}{2\sqrt{V_{\rm bi}-V}}\right), \end{aligned} \tag{9}$$

$$\begin{aligned} \frac{1}{(R_0A)_{\rm BTB}} &= \frac{q^3E(V=0)}{4\pi^2\hbar^2}\left(\frac{2m_{\rm e}}{E_{\rm g,100\%}}\right)^{1/2} \\ &\times \exp\left(-\frac{4E_{\rm g,100\%}}{3q\hbar}\sqrt{\frac{\varepsilon_{\rm SL}\varepsilon_0 m_{\rm e}}{N_{\rm red}}}\right), \end{aligned} \tag{10}$$

where $d_{\rm p,n}$ is the region thickness of the carrier, $L_{\rm e,h}$ is the carrier diffusion length, $E_{\rm g,100\%}$ is the energy gap with the 100% cutoff wavelength at 77 K, ε_0 is the vacuum permittivity, $\varepsilon_{\rm SL}$ is the static dielectric constant of the InAs/GaSb superlattices, $N_{\rm red}$ is the reduced carrier concentration ($1/N_{\rm red} = 1/N_{\rm A} + 1/N_{\rm D}$) and

$$B = \frac{4\sqrt{2m_{\rm e}(E_{\rm g}-E_{\rm t})^3}}{3q\hbar\sqrt{(2qN_{\rm A}/\varepsilon_0\varepsilon_{\rm SL})}}. \tag{11}$$

2.2. Absorption coefficient

The absorption calculated at normal incidence with the light polarized along the layer plane (TE mode) is proportional to the probability of finding the electron and the hole at the same place. The simulation is taken under the Kane four-band model,[17–19] when we consider effects of the conduction band, the heavy hole band, the light hole band and the spin–orbit band. The absorption coefficient of the superlattice is given by

$$\alpha(\hbar\omega) = \frac{K_{\rm g}}{n_{\rm b}\hbar\omega}\sum_{n,m} I_{hm}^{en}\int_0^\infty {\rm d}E_{\rm t}|\hat{e}\cdot p_{\rm cv}|^2\rho_{\rm r}^{\rm 2D} \times \frac{(1/\pi)(\hbar/\tau_{\rm in})}{(E_{hm}^{en}(0)+E_{\rm t}-\hbar\omega)+(\hbar/\tau_{\rm in})^2} \times [f_{\rm v}^m(E_{\rm t})-f_{\rm c}^n(E_{\rm t})], \quad (12)$$

where $n_{\rm b}$ is the refractive index of the superlattice, ω is the incident light angular frequency, n denotes the n-th conduction subband, m denotes the m-th valence subband, I_{hm}^{en} is the envelope function overlap integral of conduction and valence band, $|\hat{e}\cdot p_{\rm cv}|^2$ is the square momentum matrix element, $\rho_{\rm r}^{\rm 2D}$ is the two-dimensional (2D) joint density of states, $\tau_{\rm in}$ is the intraband relaxation time, $E_{hm}^{en}(0)$ is the transition energy between conduction and valence subbands at $k_{\rm t}=0$, $f_{\rm c}^n$ and $f_{\rm v}^m$ are the Fermi–Dirac distribution for the n-th conduction subband and the m-th valence subband, respectively and

$$K_{\rm g} = \frac{\pi q^2\hbar}{c_0\varepsilon_0 m_0^2}, \quad (13)$$

where c_0 is the speed of light in vacuum.

To account for the finite lifetime of excitons, the expression for α has been convoluted with a Lorentzian broadening function. The 3-to-1 intensity ratio between the heavy hole and the light hole exciton, arising from the polarization of the light, is contained in the $|\hat{e}\cdot p_{\rm cv}|^2$ factor.

As a photovoltaic structure, we focus on the situation of zero bias when it works and a uniform Fermi level is used for both conduction and valence bands. For the $\rm p^+pn^+$ superlattices, the Fermi level is determined by the doping density according to the equations given by[20]

$$N_{\rm D} = \frac{1}{A}\sum_\sigma\sum_m\sum_{k_{\rm t}} f_m^\sigma(k_{\rm t}),$$
$$N_{\rm A} = \frac{1}{A}\sum_\sigma\sum_{\rm n}\sum_{k_{\rm t}} [1-f_{\rm n}^\sigma(k_{\rm t})], \quad (14)$$

where A is the area of the active region, $k_{\rm t}$ is the wavenumber in the direction parallel to the growth direction, σ represents the upper and lower blocks since the 8×8 Hamiltonian is block-diagonalized into two 4×4 blocks through the axial approximation.

2.3. Quantum efficiency

According to the one-dimensional model deduced from the current continuity equation developed by Hovel,[21] the quantum efficiency of a pin photodetector generally has three components. These components arise from the contribution of three regions: the neutral n region, the neutral p region and the depletion region. Assuming the surface recombination velocity is zero, the quantum efficiency in three regions can be obtained respectively as follows:

$$\eta_{\rm n} = (1-R)\frac{\alpha L_{\rm h}}{(\alpha L_{\rm h})^2-1}\left\{\frac{\alpha L_{\rm h}-\exp(-\alpha d_{\rm n})\sinh(d_{\rm n}/L_{\rm h})}{\cosh(d_{\rm n}/L_{\rm h})}-\alpha L_{\rm h}\exp(-\alpha d_{\rm n})\right\}, \quad (15)$$

$$\eta_{\rm p} = (1-R)\frac{\alpha L_{\rm e}}{(\alpha L_{\rm e})^2-1}\exp(-\alpha(d_{\rm n}+d_{\rm dep}))\left\{\frac{-\alpha L_{\rm e}\exp(-\alpha x_{\rm p})-\sinh(d_{\rm p}/L_{\rm e})}{\cosh(d_{\rm p}/L_{\rm e})}+\alpha L_{\rm e}\right\}, \quad (16)$$

$$\eta_{\rm dep} = (1-R)\{\exp(-\alpha d_{\rm n})-\exp(-\alpha(d_{\rm n}+d_{\rm dep}))\}, \quad (17)$$

where R is the reflection coefficient of the superlattice–air interface and is approximately taken to be 0.34.[22] Then the total quantum efficiency can be written as

$$\eta_{\rm total} = \eta_{\rm n}+\eta_{\rm p}+\eta_{\rm dep}. \quad (18)$$

This means that the quantum efficiency will not exceed 66% at the most. Hence an antireflective coating at the entrance surface of the detector is needed to further improve the quantum efficiency.

Finally, all the basic material parameters used in these calculations for MWIR InAs/GaSb superlattices are listed in Table 1.

Table 1. Material parameters for the calculation of MWIR photodetectors.

Parameter	Symbol (unit)	Value
Donor concentration	$N_{\rm D}$ (cm^{-3})	1×10^{18}
Activated trap density	$N_{\rm t}$ (cm^{-3})	2.8×10^{11}
Generation recombination lifetime	$\tau_{\rm gr}$ (s)	3.3×10^{-8}
Intraband relaxation time	$\tau_{\rm in}$ (s)	6.58×10^{-14}
Refractive index	$n_{\rm b}$	3.8
Static dielectric constant	$\varepsilon_{\rm SL}$	15.42

3. Results and discussion

In Fig. 1, we show the calculated band structure along high symmetry directions in the entire first Brillouin zone at 77 K. The effective electron and hole masses for carriers used in this calculation are taken as: $m_{\rm e,InAs} = 0.027m_0$, $m_{\rm h,InAs} = 0.41m_0$, $m_{\rm e,GaSb} = 0.045m_0$, and $m_{\rm h,GaSb} = 0.4m_0$. The band gap of 8 ML/8 ML InAs/GaSb superlattices is 0.252 eV, with the cutoff wavelength being 4.9 μm. The calculations agree well with the reported experimental results within a certain growth uncertainty.[7,23]

Current–voltage characteristics are simulated for both the unintentionally doped reference sample and photodetectors with different p-doping concentrations at 77 K and the results are shown in Fig. 2. We can see that the total dark current is suppressed with the active region p-doped slightly and begins to deteriorate with further increased doping concentration. The first suppression comes from the fact that the diffusion current decreases with increased doping concentration due to the reduced minority carrier density; besides, the depletion width also decreases, thus lowering the generation–recombination current. However, when the doping concentration is large enough, the trap-assisted tunneling and the band-to-band tunneling terms come to play a dominant role, hence leading to the sharp increase of the dark current.

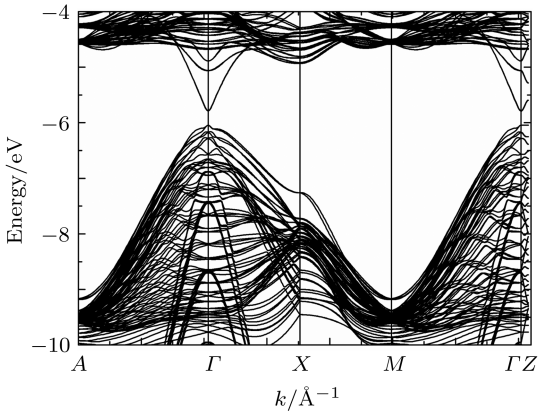


Fig. 1. Band structure of 8 ML/8 ML InAs/GaSb superlattices along high symmetry directions in the entire first Brillouin zone.

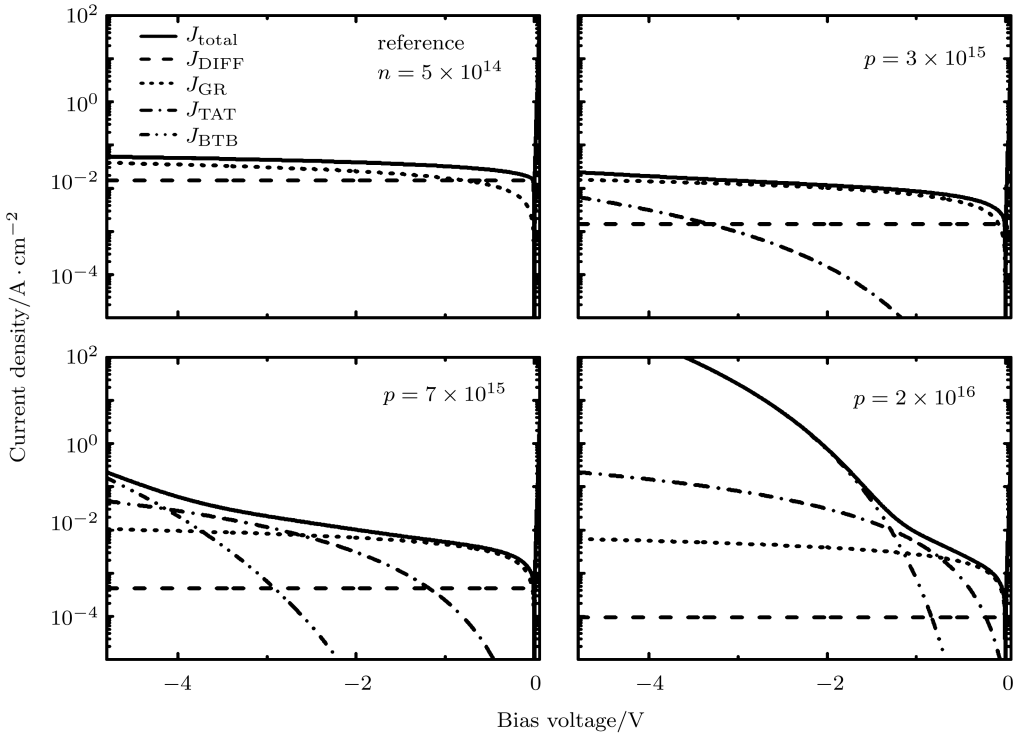


Fig. 2. Simulated current density of the reference sample and beryllium doped samples. The reference sample is modeled as p^+n and doped samples treated as n^+p.

The reduced diffusion and generation–recombination current would increase their contribution to R_0A product. In comparison with the reference sample, the differential resistance can be improved by almost one order of magnitude when doping slightly p-type in the active region. This is shown in Fig. 3 and it predicts the differential resistance as a function of the temperature. In our calculations, we ignore the Zener-tunneling-limited R_0A, which is much higher and thus does not limit the performance of the diode. Figure 3 implies that there are different dark current mechanisms which are dominant in different temperature regions. When the temperature is below 70 K, the diode is temperature-insensitive trap-limited; from 70 K to 130 K, thermally generated carriers produce a strong generation–recombination current which overwhelms the others; above 130 K, the device performance is limited by the diffusion current.

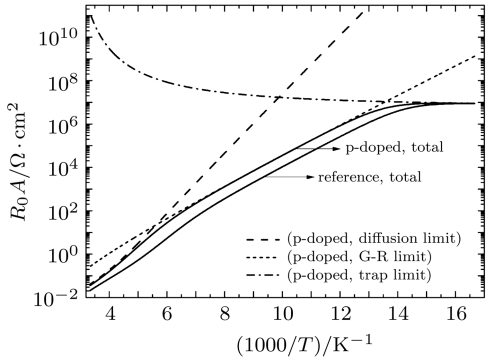


Fig. 3. Theoretical prediction of the differential resistance as a function of temperature for both the reference and doped samples.

Considering different p-doping concentrations in the active region, we polt their relationship with R_0A in Fig. 4. The diffusion and generation–recombination terms, which are both proportional to the doping concentration, are the two competing factors to the R_0A when the doping concentration is below 8×10^{16} cm^{-3}. By further increasing the doping, the maximum electric field in the depletion region enhances greatly, which results in the increased electron tunneling probability and hence the sharply decreased differential resistance.

We also studied the influences of the doping level on the optical properties of the device. Figure 5 shows the absorption coefficient as a function of the p-doping density. Apart from the absorption peak corresponding to the transition between fundamental electron and heavy-hole minibands (C1-VH1), there are two other peaks in the spectrum due to excited transitions C1-VL1 and C1-VH2, which associate the lowest electron miniband to the light-hole miniband and to the second heavy-hole miniband, respectively. As shown in Fig. 5, the doping density has almost no effect on the absorption coefficient when it is below 1×10^{17} cm^{-3}. However, once the doping density exceeds 1×10^{17} cm^{-3}, the absorption coefficient begins to decrease due to the band filling effect.[24] This can be understood by the Fermi energy lying in the valence band for heavy p-type doping density, which leads to the decrease in the number of available final states and the filled states therefore block optical excitation.

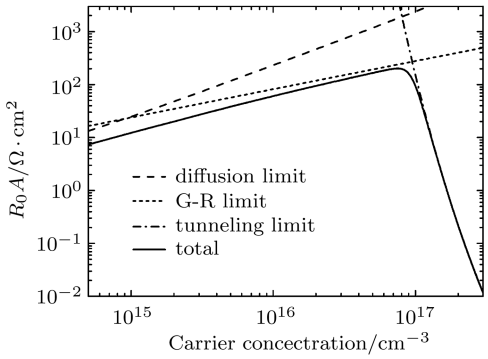


Fig. 4. Theoretical simulation of differential resistance at zero bias voltage at 77 K for doped samples.

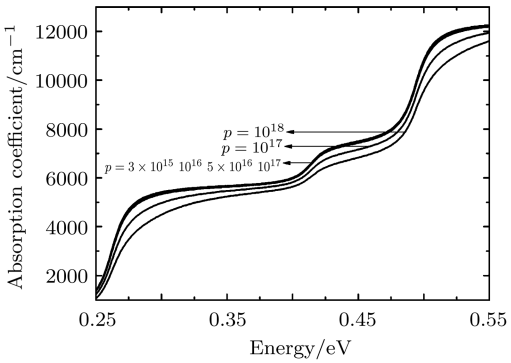


Fig. 5. Simulated absorption spectra of 8 ML/8 ML InAs/GaSb superlattices with different p-doping concentrations.

The quantum efficiency can be determined by the absorption coefficient, the diffusion length of minority carriers and the total thickness of the active region. In our simulations, layer thicknesses for all samples are the same. Both the absorption coefficient and the minority diffusion length are the function of doping concentrations. Figure 6 implies that the quantum efficiency stays almost unchanged when the doping density is below 1×10^{16} cm^{-3} and begins to decrease as the doping density further increases. This is because the depletion region shrinks with increasing doping density as well as the decrease of absorption coefficient caused by the band filling effect.

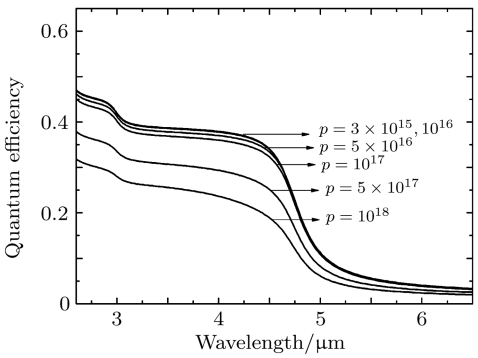


Fig. 6. Modeled quantum efficiency with different p-doping concentrations at 300 K.

4. Conclusions

We have investigated the electrical and optical properties of MWIR InAs/GaSb superlattice photodetectors as a function of the active region p-doping density. By switching the background from residual n-type to slight p-type, the electrical properties have been improved greatly. However, both the dark current and the differential resistance would begin to deteriorate by further enhancing the p-doping concentration, which is the result of the increasing tunneling mechanism. The absorption coefficient and quantum efficiency would stay almost unchanged when the doping concentration is relatively small and the optical properties get worse seriously once the doping density exceeds 1×10^{17} cm^{-3}. To make a compromise between the electrical and optical properties, we find that slightly p-doping the active region to the 3×10^{15} cm^{-3} level would improve the overall performance of the structure.

References

[1] Smith D L and Mailhiot C 1987 *J. Appl. Phys.* **62** 2545

[2] Burkle L and Fuchs F, ed. Mohamed Henini and Mahijeh Razeghi 2002 *Handbook of Infrared Detection Technologies* (UK: Elsevier) p. 159

[3] Grein C H, Young P M, Flatte M E and Ehrenreich H 1995 *J. Appl. Phys.* **78** 7143

[4] Mohseni H, Litvinov V I and Razeghi M 1998 *Phys. Rev.* B **58** 15378

[5] Darin Hoffman and Binh-Minh Nguyen 2007 *Appl. Phys. Lett.* **91** 143507

[6] Manijeh Razeghia and Binh-Minh Nguyen 2009 *Proc. SPIE* **7467** 74670T-1

[7] Wang G W, Xu Y Q, Guo J, Tang B, Ren Z W, He Z H and Niu Z C 2010 *Chin. Phys. Lett.* **27** 077305

[8] Yajun Wei and Manijeh Razeghi 2004 *Phys. Rev.* B **69** 085316

[9] Mohseni H, Wojkowski J S, Tahraoui A and Razeghi M 2000 *Proc. SPIE* **3948** 153

[10] Reine M B, Sood A K and Tredwell T J, ed. Willardson R K and Beer A C 1981 *Photovoltaic Infrared Detectors, in Semiconductors and Semimetals* Vol. 18 (New York: Academic)

[11] Yang Q K, Fuchs F, Schmitz J and Pletschen W 2002 *Appl. Phys. Lett.* **81** 4757

[12] Wong J Y 1980 *IEEE Trans. Electron. Dev.* **ED-27** 48

[13] Kinch M A 1982 *J. Vac. Sci. Technol.* **21** 215

[14] Liu E K, Zhu B S and Luo J S 2003 *Semiconductor Physics* 6th edn. (Beijing: Electronics Industry Press) (in Chinese) p. 123

[15] Pellegrino J and DeWames R 2009 *Proc. SPIE* **7298** 72981U-1

[16] Mohseni M, Wojkowski J S, Tahraoui A and Razeghi M 2000 *Proc. SPIE* **3948** 153

[17] Kane E O 1966 *The k·p Method, in Semiconductors and Semimetals* Vol. 1 (New York: Academic)

[18] Chuang S L 1995 *Physics of Optoelectronic Devices* (New York: John-Wiley)

[19] Huang J L, Wei Y, Ma W Q, Yang T and Chen L H 2010 *Acta Phys. Sin.* **59** 3099 (in Chinese)

[20] Liu G and Chuang S L 2002 *Phys. Rev.* B **65** 1652201

[21] Hovel H J 1975 *Semiconductors and Semimetals* (New York: Academic) Vol. 11 pp. 15–23

[22] Manijeh Razeghi and Darin Hoffman 2009 *Proc. IEEE* **97** 1506

[23] Rodriguez J B and Christol P 2005 *Physica* E **28** 128

[24] Bennett B R, Soref R A and Alamo J A D 1990 *IEEE Journal of Quantum Electronics* **26** 113